Polymer 50 (2009) 4228–4240

Contents lists available at ScienceDirect

Polymer

journal homepage: www.elsevier.com/locate/polymer

Effect of processing on the crystalline orientation, morphology, and mechanical properties of polypropylene cast films and microporous membrane formation

Seyed H. Tabatabaei, Pierre J. Carreau*, Abdellah Ajji

CREPEC, Chemical Engineering Department, Ecole Polytechnique, C.P. 6079, Succ. Centre ville, Montreal, QC H3C 3A7, Canada

ARTICLE INFO

Article history:
Received 30 March 2009
Received in revised form
19 June 2009
Accepted 28 June 2009
Available online 3 July 2009

Keywords:
Linear polypropylene
Crystallization
Morphology

ABSTRACT

Cast films of a high molecular weight linear polypropylene (L-PP) were prepared by extrusion followed by stretching using a chill roll. An air knife was employed to supply air to the film surface right at the exit of the die. The effects of air cooling conditions, chill roll temperature, and draw ratio on the crystalline orientation, morphology, mechanical and tear properties of the PP cast films were investigated. The crystallinity and crystal size distribution of the films were studied using differential scanning calorimetry (DSC). It was found that air blowing on the films contributed significantly to the uniformity of the lamellar structure. The orientation of crystalline and amorphous phases was measured using wide angle X-ray diffraction (WAXD) and Fourier transform infrared (FTIR). The amount of lamellae formation and long period spacing were obtained via small angle X-ray scattering (SAXS). The results showed that air cooling and the cast roll temperature have a crucial role on the orientation and amount of lamellae formation of the cast films, which was also confirmed from scanning electron microscopy (SEM) images of the films. Tensile properties and tear resistance of the cast films in machine and transverse directions (MD and TD, respectively) were evaluated. Significant increases of the Young modulus, yield stress, tensile strength, and tensile toughness along MD and drastic decreases of elongation at break along TD were observed for films subjected to air blowing. Morphological pictograms are proposed to represent the molecular structure of the films obtained without and upon applying air cooling for different chill roll temperatures. Finally, microporous membranes were prepared from annealed and stretched films to illustrate the effect of the PP cast film microstructure on the morphology and permeability of membranes. The observations of SEM surface images and water vapor transmission rate of the membranes showed higher pore density, uniform pore size, and superior permeability for the ones obtained from the precursor films prepared under controlled air cooling.

1. Introduction

Among a wide range of resins, polypropylene (PP) is a well-known semicrystalline polymer and, in comparison with polyethylene (PE), PP has a higher melting point, lower density, higher chemical resistance, and better mechanical properties, which make it useful for many industrial applications.

The crystalline phase orientation in semicrystalline polymers such as polypropylene enhances many of their properties particularly mechanical, impact, barrier, and optical properties [1]. Obtaining an oriented structure in PP is of great interest to many processes such as film blowing, fiber spinning, film casting, and etc. In these processes the polymer melt is subjected to shear (in the die) and elongational (at the die exit) flow and crystallize during or subsequent to the imposition of the flow.

It is well-known that strain under flow strongly enhances the crystallization kinetics and allows the formation of a lamellar structure instead of the spherulitic one. The effect of flow on crystallization is called flow induced crystallization (FIC) while the flow can be shear, extensional or both [2]. FIC molecular models show that flow induces orientation of polymer chains, resulting in enhancement of the nucleation rate [2–4]. Under flow, two major types of crystallization can occur, depending on the magnitude of the stress [1]: low stress results in twisted lamellae, while high stress produces a shish–kebab structure in which the lamellae grow radially on the shish without twisting [1].

Similar to shear flow, it has also been reported that extensional flow promotes fibrillar like structure oriented in the flow direction that serves as nucleation for radial growth of chain-folded lamellae perpendicular to the stress direction [5].

The effects of material parameters on shear induced crystallization process for PP have been investigated using in-situ small angle X-ray scattering (SAXS) and/or wide angle X-ray diffraction (WAXD) analyses [6–8]. Agarwal et al. [6] examined the influence of long

* Corresponding author. Tel.: +1 514 340 4711x4924; fax: +1 514 340 2994.
E-mail address: pcarreau@polymtl.ca (P.J. Carreau).

0032-3861/$ – see front matter © 2009 Published by Elsevier Ltd.
doi:10.1016/j.polymer.2009.06.071

chain branches on the stress-induced crystallization. Adding a certain level of branches improved the orientation of the crystal blocks and the crystallization kinetics due to the longer relaxation time and the molecular structure. Somani et al. [7] followed the orientation development upon applying different shear rates. They found that, at a certain shear rate, only molecules with a chain length (molecular weight) above a critical value (critical orientation molecular weight, M_c) can form stable oriented row nuclei (shish). The shorter chains create lamellae over these nuclei sites. In another study, Somani et al. [8] compared the oriented microstructure under shear flow of isotactic polypropylene melts (PP-A and PP-B) with the same number average molecular weight but different molecular weight distribution (MWD). The amount of the high molecular weight species was larger in PP-B than in PP-A. Their results showed that the shish structure evolved much earlier for PP-B, which had more pronounced crystal orientation and faster crystallization kinetics. They concluded that even a small increase in the concentration of the high molecular weight chains led to a significant increase in the shish or nuclei site formation. In our recent study [9], addition of up to 10 wt% of a high molecular weight component to a low molecular weight one enhanced the formation of the row nucleated structure probably due to an increase in the nucleating sites.

The crystallization behavior of semicrystalline polymers is significantly influenced by the process conditions. Under quiescent isothermal crystallization, the size of the spherulites, the degree of crystallinity, and the kinetics depend on temperature, while in quiescent non-isothermal conditions, both temperature and cooling rate are important factors [2].

Numerous studies have focused on the structure of PE and PP blown films using various materials under different processing conditions. However, as far as we know no experimental study has been conducted on the cast film process with emphasis on the effect of cooling using a chill roll and/or air. Therefore, the main objective of this work is to elucidate the effect of air cooling, in addition to the other process conditions (i.e. chill roll temperature and draw ratio), on the flow induced crystallization and orientation developed in PP cast films. We also report results on the tear properties and mechanical behavior of the cast films and the properties of the membranes produced from these films. This is the first effort to address this issue from a structural point of view.

2. Experimental

2.1. Material

A commercial linear polypropylene (PP5341) supplied by ExxonMobil Company was selected. It had a melt flow rate (MFR) value of 0.8 g/10 min (under ASTM conditions of 230 °C and 2.16 kg). Its molecular weight was estimated from the relationship between the zero-shear viscosity and the molecular weight [10] and found to be around 772 kg/mol. The resin showed a polydispersity index (PDI) of 2.7, as measured using a GPC (Viscotek model 350) at 140 °C and 1,2,4-trichlorobenzene (TCB) as a solvent. Its melting point, T_m, and crystallization temperature, T_c, obtained from differential scanning calorimetry at a rate of 10 °C/min, were 161 °C and 118 °C, respectively.

2.2. Film and membrane preparation

The cast films were prepared using an industrial multilayer cast film unit from Davis Standard Company (Pawcatuck, CT) equipped with a 2.8 mm thick and 122 cm width slit die and two cooling drums. The extrusion was carried out at 220 °C and the distance between the die exit to the nip roll was 15 cm. The die temperature was set at 220 °C and draw ratios of 60, 75, and 90 were applied. An air knife with dimensions of 3 mm opening and 130 cm width was mounted close to the die to provide air to the film surface right at the exit of the die. The variables of interest were chill roll temperature, amount of air flow, and draw ratio. The films were produced under chill roll temperatures of 120, 110, 100, 80, 50, and 25 °C. For all the cast roll temperatures, the air cooling rates used were 0, 1.2, 7.0, and 12 L/s. These air cooling conditions are noted as: no air flow rate (N-AFR), low air flow rate (L-AFR), medium air flow rate (M-AFR), and high air flow rate (H-AFR), respectively.

For membrane fabrication, the precursor films with a thickness, width and length of 35 μm, 46 mm, and 64 mm, respectively, were used. The films were first annealed at 140 °C for 30 min and then cold and hot stretched at 25 °C and 120 °C, respectively. Both annealing and stretching were performed using an Instron machine equipped with an environmental chamber. A drawing speed of 50 mm/min was applied during cold and hot stretching steps. The details for the fabrication of the microporous membranes can be found elsewhere [9].

2.3. Film and membrane characterization

2.3.1. Fourier transform infrared spectroscopy (FTIR)

For FTIR measurements, a Nicolet Magna 860 FTIR instrument from Thermo Electron Corp. (DTGS detector, resolution 2 cm^{-1}, accumulation of 128 scans) was used. The beam was polarized by means of a Spectra-Tech zinc selenide wire grid polarizer from Thermo Electron Corp. The measurement is based on the absorption of infrared light at certain frequencies corresponding to the vibration modes of atomic groups present within the molecule. In addition, if a specific vibration is attributed to a specific phase, the orientation within that phase can be determined [11]. If the films are oriented, the absorption of plane-polarized radiation by a vibration in two orthogonal directions, specifically parallel and perpendicular to a reference axis (MD), should be different. The ratio of these two absorption values is defined as the dichroic ratio, D [11]:

$$D = \frac{A_{\parallel}}{A_{\perp}} \tag{1}$$

where $A_{\parallel}$ is the absorption parallel and $A_{\perp}$ is the absorption perpendicular to a specific reference axis. The Herman orientation function of this vibration is obtained according to Ref. [11]:

$$f = \frac{D-1}{D+2} \tag{2}$$

For polypropylene, absorption at the wavenumber of 998 cm^{-1} is attributed to the crystalline phase (c-axis) while absorption at the wavenumber of 972 cm^{-1} is due to the contribution of both crystalline and amorphous phases. From the former absorption, the orientation of the crystalline phase, f_c, can be determined while from the latter, the average orientation function, f_{av}, is obtained. The orientation of the amorphous phase, f_{am}, can be calculated according to:

$$f_{av} = X_c f_c + (1 - X_c) f_{am} \tag{3}$$

where X_c is the degree of the crystallinity. Using FTIR, the global, crystalline and amorphous orientations can be determined.

2.3.2. X-ray diffraction

XRD measurement was carried out using a Bruker AXS X-ray goniometer equipped with a Hi-STAR two-dimensional area detector. The generator was set up at 40 kV and 40 mA and the copper CuKα radiation ($\lambda = 1.542$ Å) was selected using a graphite crystal monochromator. The sample to detector distance was fixed at 9.2 cm for wide angle diffraction and 28.2 cm for small angle

X-ray scattering analysis. To get the maximum diffraction intensity several film layers were stacked together to obtain the total thickness of about 2 mm.

Wide angle X-ray diffraction (WAXD) is based on the diffraction of a monochromatic X-ray beam by the crystallographic planes (*hkl*) of the polymer crystalline phase. Using a pole figure accessory, the intensity of the diffracted radiation for a given *hkl* plane is measured as the sample is rotated through all possible spherical angles with respect to the beam. This gives the probability distribution of the orientation of the normal to *hkl* plane with respect to the directions of the sample.

The Herman orientation function of a crystalline axis is given by [12]:

$$f = \frac{(3\cos^2\phi - 1)}{2} \tag{4}$$

where ϕ is the angle between the unit cell axes (a, b, and c) and reference axes. Details about the calculations can be found elsewhere [12].

The orientation factors from WAXD are mainly due to the crystalline part, therefore no information about the orientation of the amorphous phase can be obtained. Small angle X-ray scattering (SAXS) was used to compare the level of the lamellae formation for the different samples and to estimate the long period between lamellae.

2.3.3. Thermal analysis

Thermal properties of specimens were analyzed using a TA instrument differential scanning calorimeter (DSC) Q 1000. The thermal behavior of films was obtained by heating from 50 to 220 °C at a heating rate of 10 °C/min. The reported crystallinity results were obtained using a heat of fusion of 209 J/g for fully crystalline polypropylene (PP) [13].

2.3.4. Mechanical and tear analysis

Tensile tests were performed using an Instron 5500R machine equipped with an environmental chamber for tests at high temperature. The procedure used was based on the D638-02a ASTM standard. A standard test method for the tear resistance of plastic films based on ASTM D1922 was used to obtain the MD and TD tear resistances. According to this standard, the work required in tearing is measured by the loss of energy of the encoder, which measures the angular position of the pendulum during the tearing operation.

2.3.5. Morphology

To clearly observe the crystal arrangement of the PP cast films, an etching method was employed to remove the amorphous part. The PP films were dissolved in a 0.7% solution of potassium permanganate in a mixture of 35 volume percentage of orthophosphoric and 65 volume percentage of sulfuric acid. The potassium permanganate was slowly added to the sulfuric acid under rapid agitation. At the end of the reaction time, the samples were washed as described in Olley and Bassett [14].

A field emission scanning electron microscope (FESEM- Hitachi S4700) was employed for the observation of the etched films surfaces as well as microporous membranes. This microscope provides high resolution of 2.5 nm at a low accelerating voltage of 1 kV and high resolution of 1.5 nm at 15 kV with magnification from 20× to 500kx.

2.3.6. Water vapor transmission

The permeability to water vapor was measured via a MOCON PERMATRAN-W Model 101K at room temperature. It is composed of three chambers: an upper chamber containing liquid water and separated from the center chamber by two porous films. Water vapor diffuses from the first film to fill the space between the films to reach 100% relative humidity (RH). The center chamber is separated from the lower one by the test film. The diffused vapor is swept away by N_2 gas to a relative humidity (RH) sensor.

2.4. Rheological characterization

Dynamic rheological measurements were carried out using a Rheometric Scientific SR5000 stress controlled rheometer with a parallel plate geometry of 25 mm diameter and a gap equal to 1.5 mm at the temperatures of 180, 195, 210, and 225 °C under nitrogen atmosphere. Molded discs of 2 mm thick and 25 mm in diameter were prepared using a hydraulic press at 190 °C. Prior to frequency sweep tests, time sweep tests at a frequency of 0.628 rad/s and different temperatures were performed for two hours to check the thermal stability of the specimens. No degradation (less than 3% changes) was observed at test temperatures for the duration of the frequency sweep measurements. The dynamic data were obtained in the linear regime and used to evaluate the weighted relaxation spectra of the samples.

3. Results and discussion

We first present experimental data that clearly demonstrate the effects of process conditions, particularly air cooling and drum temperature, on crystallization, orientation of the amorphous and crystalline phases, and also tear and mechanical properties. Subsequently, two morphological pictograms are proposed to describe the observed experimental data and the reasons for these observations are discussed. Finally, the structure and properties of the microporous membranes obtained from the PP cast films having different microstructures are presented.

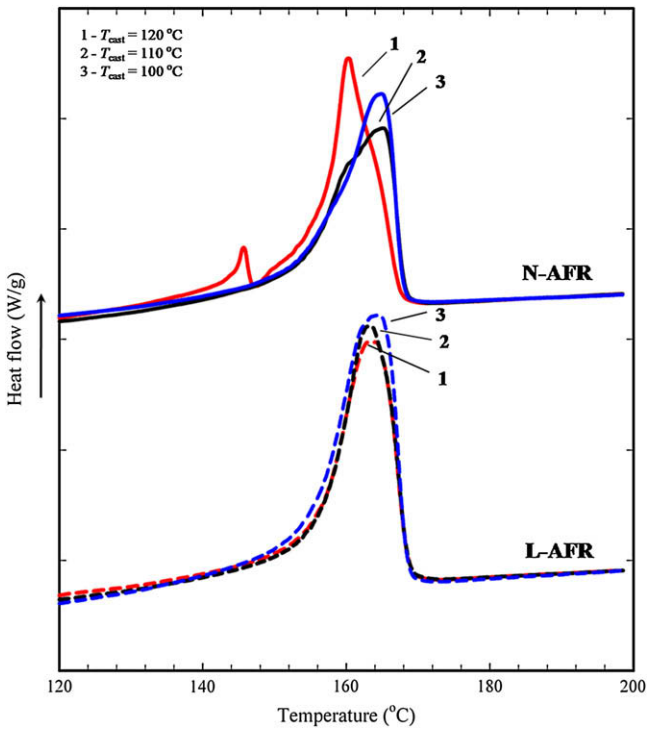

Fig. 1. DSC scans of cast films for roll temperatures of 120, 110, and 100 °C. The top curves are the thermograms of cast films produced under N-AFR condition whereas the bottom curves are the thermograms of films fabricated under L-AFR; DR = 75.

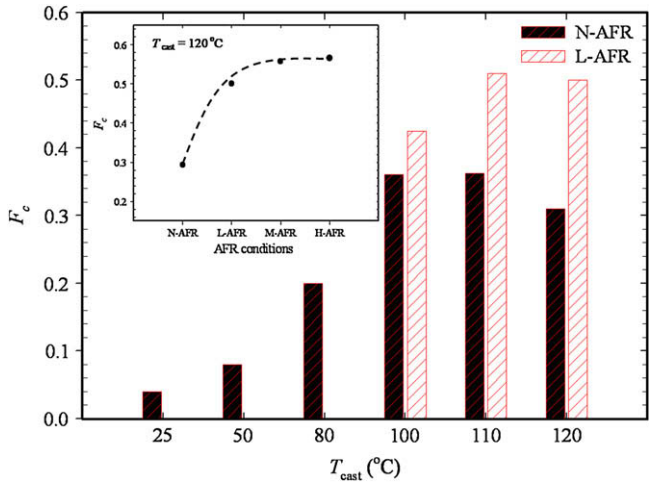

Fig. 2. Crystalline orientation functions for different cast roll temperatures. The inset is a plot of the crystalline orientation function versus the air flow rate conditions for T_{cast} = 120 °C; DR = 75.

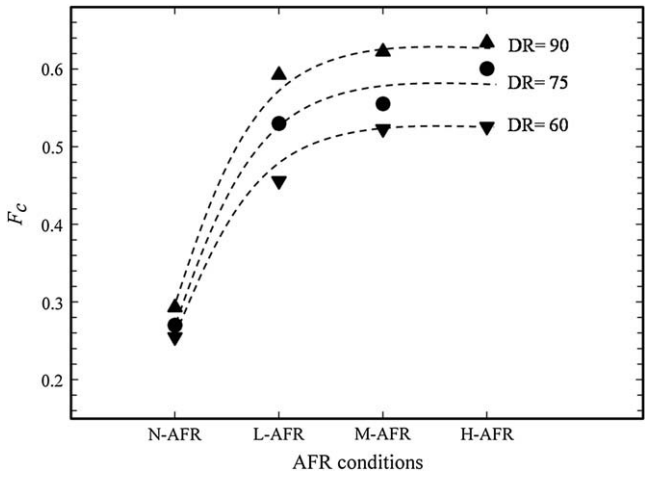

Fig. 4. Crystal orientation functions for different air flow rate conditions at draw ratios of 60, 75, and 90; T_{cast} = 120 °C.

The effects of cast roll temperature (T_{cast}) and air cooling on thermal behavior of the films were examined using differential scanning calorimetry (DSC) and the results are shown in Fig. 1. The top curves in this figure exhibit the thermograms of the films prepared at the chill roll temperatures of 100, 110, and 120 °C without air cooling. For these films, melting peaks around 163, 162, and 156 °C are observed, respectively. However, for the sample obtained at the drum temperature of 120 °C and no air flow rate condition (N-AFR) an additional peak at 144 °C is observed. Also for the sample obtained at the cast roll temperature of 110 °C a small shoulder at 156 °C is seen. These suggest the presence of a bimodal crystal (either lamellae or spherulite) size distribution (the WAXD measurements for these specimens showed no intensity peaks corresponding to the beta crystal form; therefore, the presence of this type of crystals is excluded). Both the additional peak and shoulder disappeared when T_{cast} was set at 100 °C or less (not shown). The thermograms of the films subjected to a small amount of air flow at different T_{cast} (bottom curves in Fig. 1) show narrower melting curves without any additional peak or shoulder. These indicate a more uniform crystal size structure for the films prepared at L-AFR condition.

The orientation and arrangement of the crystal lamellae in the cast films are key factors in controlling the final properties of manufactured films. Figs. 2 and 3 present the Herman orientation functions of the crystalline phase as well as of the amorphous phase obtained from FTIR, respectively. For the N-AFR condition, it is obvious that decreasing T_{cast} reduces the orientation of both the crystalline and amorphous phases (Figs. 2 and 3). For no air flow (N-AFR) and very low T_{cast}, quenching of the polymeric film happens and as a consequence a spherulitic crystal structure is expected, which leads to quite low crystal alignment. However, by increasing the drum temperature, the film temperature gets close to the crystallization point, T_c, of the resin; thus the molecules have more chance to crystallize in the extended configuration created under high draw ratio. This results in films with higher crystal orientation. Moreover, compared to the no air cooled films, significant improvement in the orientation of the crystalline and amorphous phases is observed when the film surface is exposed to a small amount of air cooling (Figs. 2 and 3). For the samples obtained under air cooling and at a drum temperature of 80 °C and lower, the orientations (not shown) were close to the one at T_{cast} of 100 °C and the reasons for that will be explained later. The insets in Figs. 2 and 3 reveal the Herman orientation functions of the crystalline and amorphous phases of the samples obtained at T_{cast} of 120 °C for

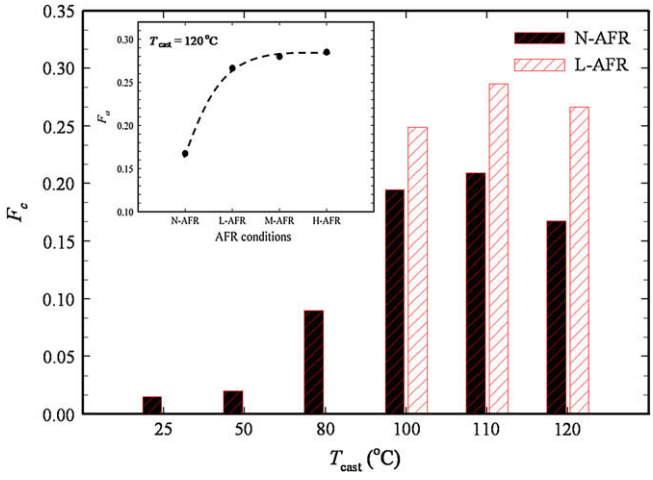

Fig. 3. Amorphous orientation functions for different cast roll temperatures. The inset is a plot of the amorphous orientation function versus the air flow rate conditions for T_{cast} = 120 °C; DR = 75.

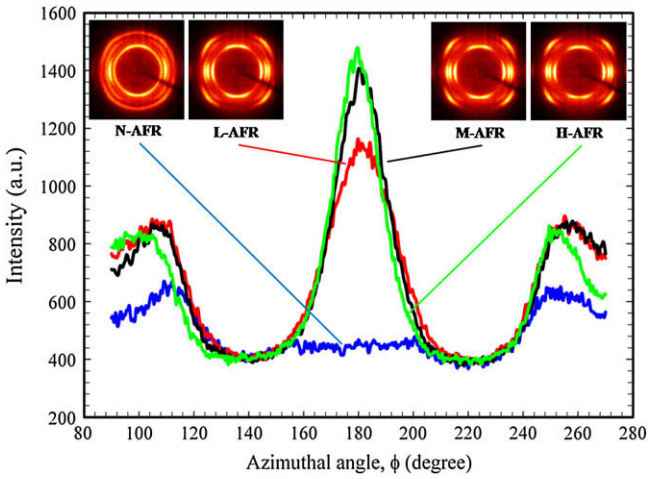

Fig. 5. 2D WAXD patterns and azimuthal intensity profiles at 2θ of the 110 refection plane of PP at different air cooling conditions; T_{cast} = 120 °C and DR = 75.

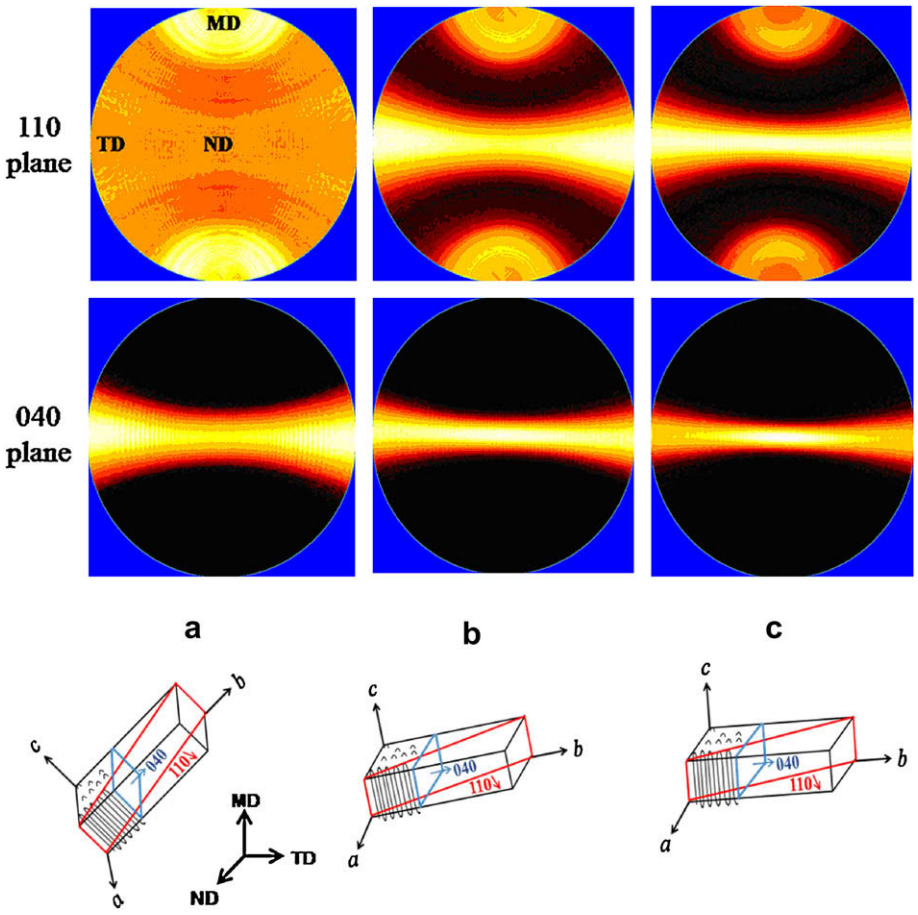

Fig. 6. Pole figures for the films obtained under different air cooling conditions. (a) N-AFR, (b) L-AFR, and (c) M-AFR; $T_{cast} = 120\ ^{\circ}C$ and DR = 75. Schematics show the assumed crystal orientation.

different air flow rates, respectively. It is clear that applying a small amount of air flow enhances the orientation of the crystalline and amorphous phases drastically while further increases in air flow do not significantly affect them.

The effect of the amount of applied strain, either in shear or elongational flow, on the lamellar structure of the various resins has been investigated recently [7,15–17]. The authors reported that as the level of strain increased, more lamellae accompanied with

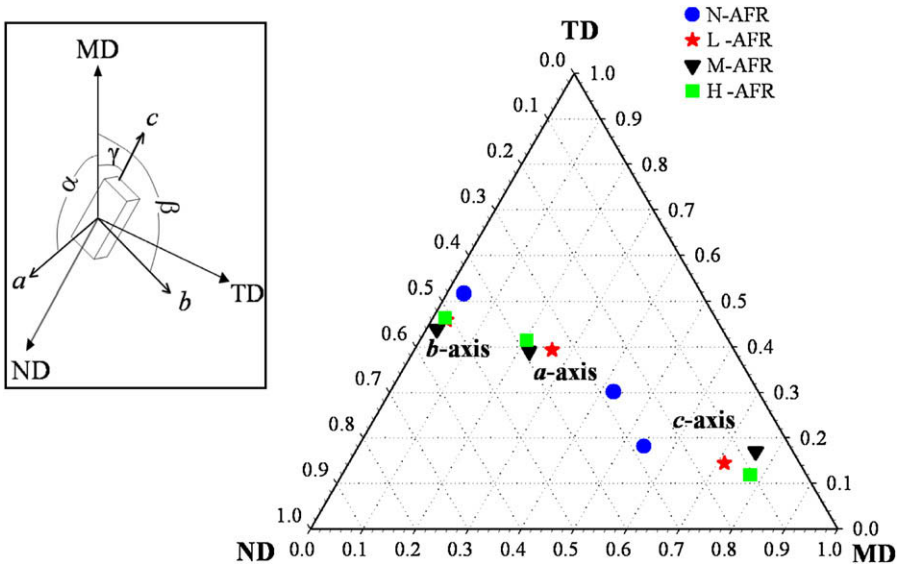

Fig. 7. Orientation characteristics as $\cos^2(\phi)$ of the crystal axes (a, b and c) along MD, TD, and ND; $T_{cast} = 120\ ^{\circ}C$ and DR = 75. The schematic represents the film production axes and crystal block coordinates.

Table 1
Crystal characteristics of the cast films obtained under different air cooling rates; DR = 75.

	FWHM (110)	D_{110}, Å	FWHM (040)	D_{040}, Å	X_c (XRD)	X_c (DSC)
T_{cast} = 120 °C, N-AFR	1.24	72	1.06	84	42.2	42.2
T_{cast} = 120 °C, L-AFR	1.14	78	0.86	103	44.3	43.2
T_{cast} = 120 °C, M-AFR	1.13	79	0.87	102	45.7	44.4
T_{cast} = 120 °C, H-AFR	1.12	80	0.87	102	46.1	44.6

better orientation were generated. The influence of draw ratio on the orientation of the crystalline and amorphous phases has also been considered [9,17,18]. In the cast film process of PP, an almost linear relationship between the draw ratio and the orientation factor was reported [9,18]. At low draw ratios, the lamellae were not well-aligned perpendicular to the flow direction, but at high draw ratios, the lamellae aligned themselves perpendicular to the machine direction, resulting in higher orientation. In this study, the influence of the draw ratio on the orientation function with and without the use of air flow is illustrated in Fig. 4 for draw ratios of 60, 75, and 90. Obviously, compared to the no air cooled films and for all the draw ratios, a jump in the orientation parameter is seen by the use of low air cooling. In addition, the draw ratio has a stronger effect on the orientation function for the films subjected to air cooling.

The effect of air cooling on orientation of the crystalline phase was also considered using WAXD, as shown in Fig. 5. In the WAXD patterns, the first and second rings represent the patterns for the 110 and 040 crystalline planes, respectively [12]. A diffraction ring is seen for the 110 crystallographic plane for the no air cooled film, indicating a low crystalline phase orientation. However, instead of rings, arcs that are sharper and more concentrated in the center are observed for the air cooled samples, implying more orientation. This behavior can be better shown when the intensity is plotted as a function of the azimuthal angle. The azimuthal angle, ϕ, is 0 or 180° along the equator and 90 or 270° along the meridian. For each ϕ, the average intensity at 2θ (=12.6° ± 0.17°) of the 110 plane was extracted from the 2D WAXD patterns and the results for the samples produced under different air flow rates are plotted in Fig. 5. Noticeable jumps at azimuthal angles around 180° as well as about 90° and 270° are observed when a small amount of air blowing is applied while further increases in the air flow rate do not dramatically impact the azimuthal intensity profile. The much sharper peaks for the air cooled films indicate a higher orientation of the crystal lamellae compared to the no air cooled ones.

The crystalline orientation can also be analyzed quantitatively from the pole figures of the 110 and 040 planes, as illustrated in Fig. 6. The normal to the 110 plane is the bisector of the *a* and *b* axes and the 040 plane is along the *b*-axis of unit crystal cells [12]. For the film obtained without air cooling, slight orientations of the 110 and 040 planes are detected in MD and TD, respectively. However, for the film produced at L-AFR a significant orientation of the 110 plane is observed along TD and that of the 040 plane (*b*-axis) is in both TD and ND. The pole figures for the samples obtained at higher air flow rates (i.e. M-AFR and H-AFR) were similar to L-AFR with slightly higher orientation intensities. The schematics in Fig. 6 represent the crystal alignments based on their pole figures.

The orientation features, in terms of $\cos^2(\phi)$ of the crystalline axes (i.e. *a*, *b*, and *c* (see the sketch in Fig. 7)) along MD, TD, and ND obtained from the Herman orientation function for the no air cooled as well as the air cooled films casted at the chill roll temperature of 120 °C are presented in the triangular plot of Fig. 7. It is obvious that a small amount of cooling causes a large shift of the *c*-axis of the crystals towards the MD, while *a*- and *b*-axes take a position closer to the TD and ND planes. This clearly shows that air cooling enhances the orientation of the films, in accordance with the FTIR data. It should be mentioned that the orientation functions obtained using FTIR were slightly larger than the values from the WAXD pole figure. The discrepancies in the values of the measured *c*-axis orientation may be due to different factors such as peak deconvolution, contribution of the amorphous phase, etc. as discussed for PE and PP elsewhere [1].

The degree of crystallinity (X_c) of the samples determined using WAXD and DSC is presented in Table 1. In WAXD, the contributions arising from the crystalline and amorphous parts were extracted via peak fitting of the 2θ diffraction pattern. Similarly to DSC results, it was observed that cooling improves crystallinity. However, the crystallinity obtained from WAXD was slightly higher than that from DSC. In addition, the average crystal width in the directions of the 110 and 040 crystallographic planes were determined from the full width at half maximum $\Delta(2\theta)$ of the deconvoluted diffraction profiles according to the following equation [19]:

$$D_{hlk} = \frac{K\lambda}{\Delta(2\theta)\cos\theta} \quad (5)$$

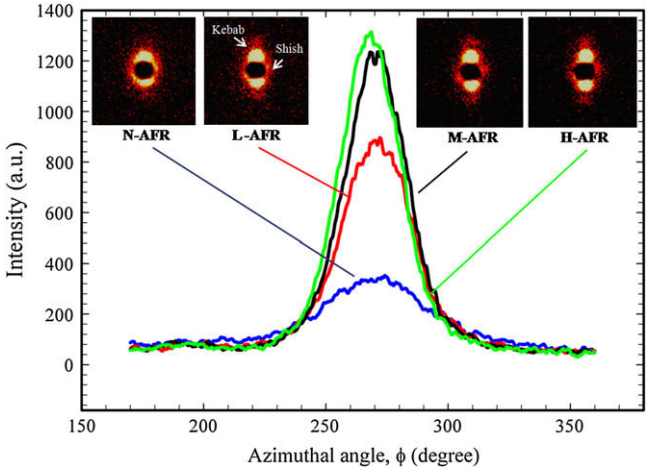

Fig. 8. 2D SAXS patterns and azimuthal intensity profiles at the meridian of PP films for different air flow cooling conditions; T_{cast} = 120 °C and DR = 75.

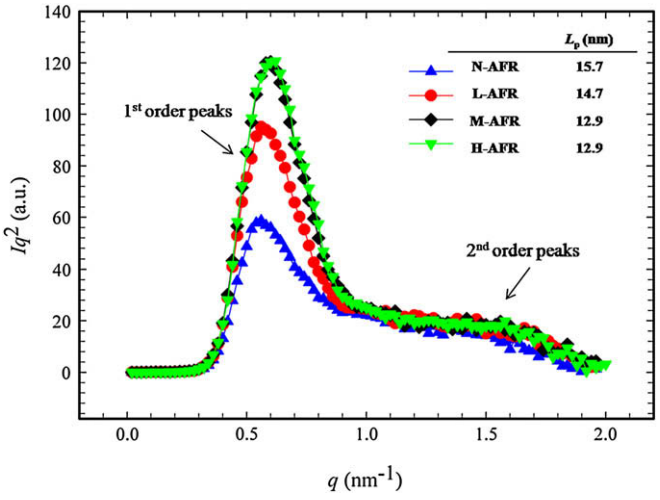

Fig. 9. Lorentz corrected SAXS intensity profiles for the films prepared under various air cooling conditions; T_{cast} = 120 °C and DR = 75.

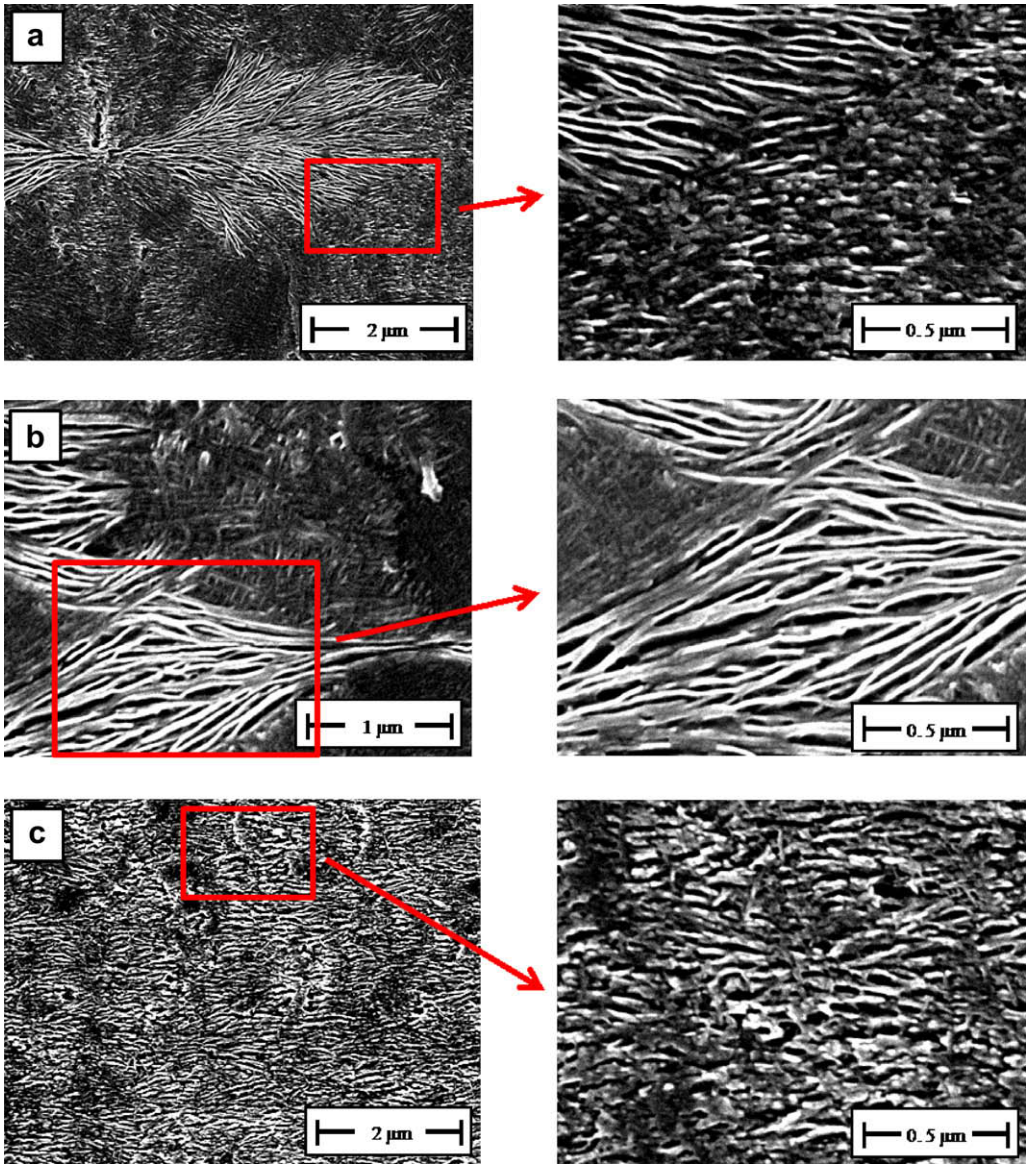

Fig. 10. SEM micrographs of the surface of films obtained under: (a) N-AFR and $T_{cast} = 120\ ^{\circ}C$, (b) N-AFR and $T_{cast} = 110\ ^{\circ}C$, and (c) L-AFR and $T_{cast} = 120\ ^{\circ}C$. The right images are high magnification micrographs of the sections corresponding to the rectangles; DR = 75. MD ↑ and TD →.

where K is a crystallite form coefficient that is taken equal to 1 and λ is the X-ray wavelength. Although it is known that this equation is not accurate because it neglects the broadening due to the lattice distortions, it allows a useful comparison of the crystalline structures for the various films. Table 1 also presents the variations of the D_{110} and D_{040} with air cooling for the films casted at 120 °C. Both

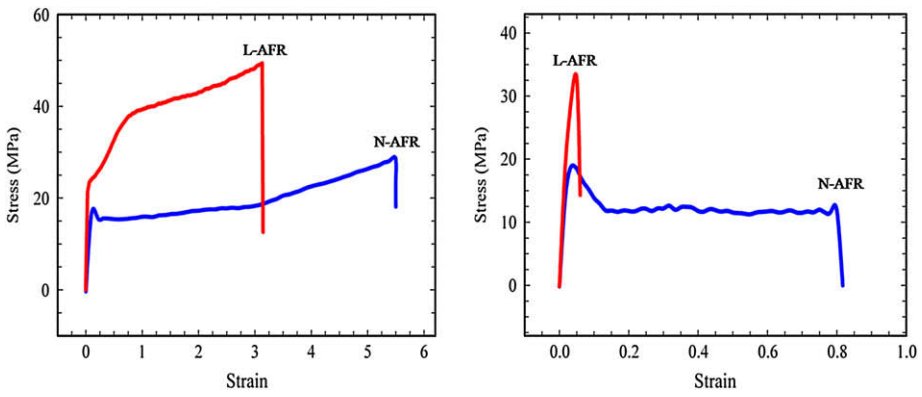

Fig. 11. Typical stress–strain behavior for the films prepared under N-AFR and L-AFR conditions along MD (left figure) and TD (right figure); $T_{cast} = 120\ ^{\circ}C$ and DR = 75.

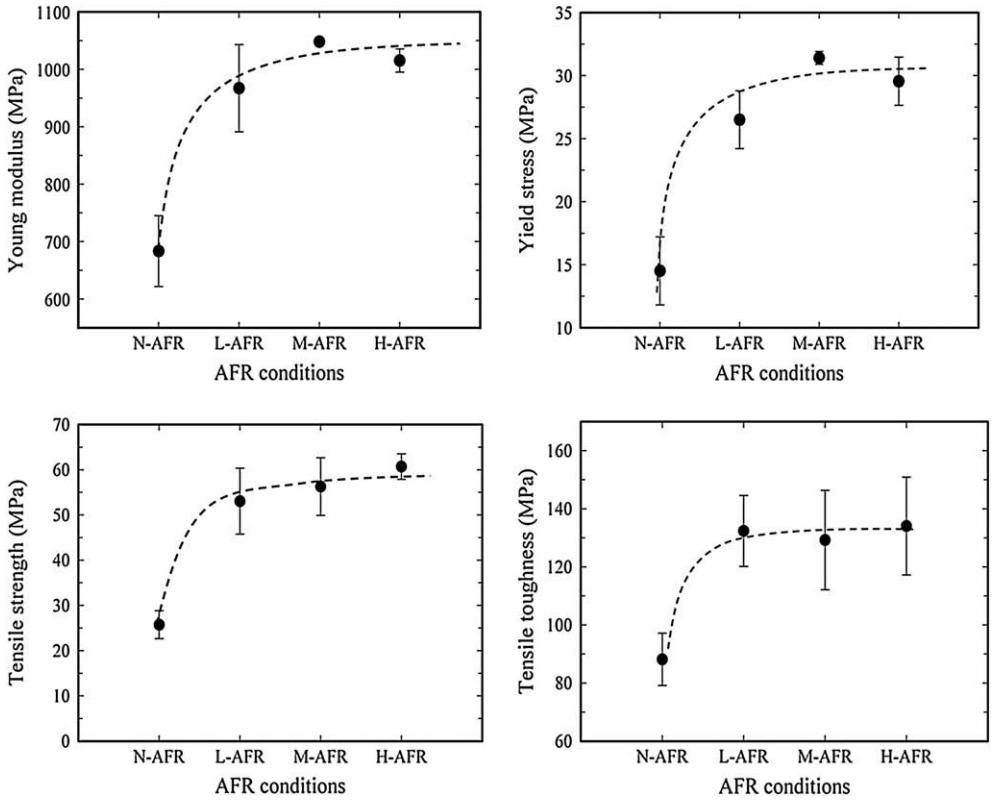

Fig. 12. Mechanical properties of the films along MD for various air flow rate conditions; $T_{cast} = 120\ ^{\circ}C$ and DR = 75.

D_{110} and D_{040} are enhanced by the use of low air cooling and do not vary by further increases of air flow. The D_{040} crystallite size corresponds to an average size of the crystallites that are oriented parallel to the film plane. Therefore, the increase of D_{040} suggests that the crystallite size is increased in a direction parallel to the *b* crystallographic axis. The effect of the cast roll temperature on the D_{040} was also evaluated (not shown here) and no noticeable impacts were found.

Fig. 8 illustrates the SAXS patterns as well as the azimuthal intensity profile for the films obtained under different air cooling rates. The equatorial streak in the SAXS patterns is attributed to the formation of the shish, while the meridian maxima are attributed to the lateral lamellae or kebabs [6]. Looking at the meridian intensity (either pattern or azimuthal profile), the formation of more lamellae for the air cooled samples is obvious. In addition, for all conditions, it is clear that the contribution of the shish to the crystalline phase is much less than that of lamellae, confirming the results of Somani et al. [20] for PE and PP.

The long period distance, L_p, was estimated from the position of the Lorentz corrected intensity maxima, as demonstrated in Fig. 9 ($L_p = 2\pi/q_{max}$ where q is the intensity vector, $q = 4\pi\sin\theta/\lambda$,). We observe a first order peak arising from stacks of parallel lamellae and a second order peak indicating that the periodicity of the lamellae is high [21]. Air cooling slightly shifts the peaks to higher values, indicating a decrease of the long period spacing. Long period spacing results for the no air cooled as well as the air cooled specimens are also reported in Fig. 9. The value of L_p for the films subjected to air cooling is smaller than that for the films produced without applying air cooling ($L_p = 14.7$ nm compared to 15.7 nm) and decreases with increasing AFR. As all films were produced

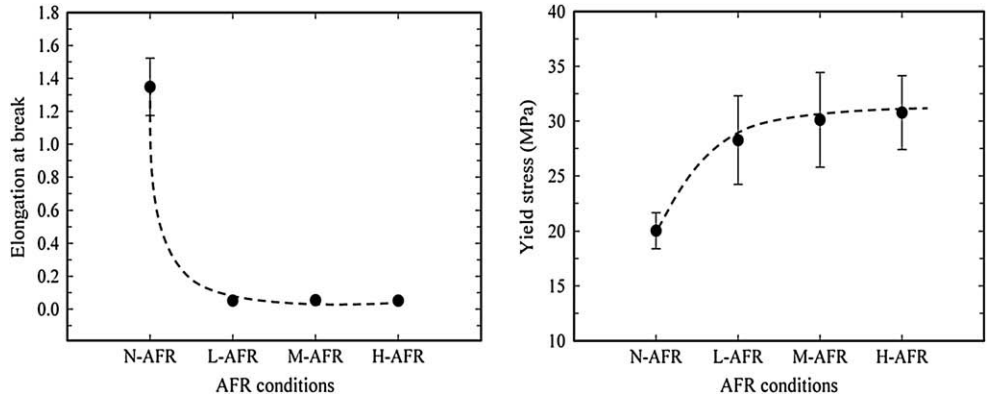

Fig. 13. Elongation at break (left figure) and yield stress (right figure) of the films along TD for various air flow rate conditions; $T_{cast} = 120\ ^{\circ}C$ and DR = 75.

under the same draw ratio, the decrease of L_p is attributed to the formation of more lamellae and consequently a more compact structure, which reduces the distance between lamellae.

The previous results imply that an oriented shish–kebab crystal structure is obtained by the use of air cooling in addition to the chill roll, compared to a much less ordered crystal structure for the no air cooled films. These differences can be clearly visualized from SEM surface images of the etched films (etching removes the amorphous region), as demonstrated in Fig. 10. Fig. 10a shows the micrograph of the surface of the film obtained without employing air cooling and at T_{cast} of 120 °C. For such conditions, spherulites, small rows of lamellae, and some cross-hatched crystalline structures coexist. The size of the spherulites is much larger than the lamellae, whereas the lamellae have been oriented somehow perpendicular to MD. The rectangle in Fig. 10a illustrates the interface of a spherulite and rows of lamellae and its higher magnification image is shown on the right. More spherulites and lamellar branching are observed for the films prepared at T_{cast} of 110 °C and without the use of air cooling (Fig. 10b). The lamellar branching from the primary lamellae is produced by epitaxial growth due to cross-hatched lamellar texture, which is a unique characteristic of PP crystalline structure [1]. The rectangle in Fig. 10b exhibits the impingement of spherulites, clearly demonstrated by its higher magnification micrograph on the right. For the no air cooling condition, the number of spherulites increased and the cross-hatched morphology became more random (balanced) (not shown) as the cast roll temperature changed from 100 °C to 25 °C. This can be explained by the quenching effect (and hence low crystal orientation) of the cast roll at temperatures much lower than T_c of the resin. In contrast, a more uniform and ordered stacked lamellar structure is observed for the films subjected to a low air cooling (Fig. 10c), confirming the FTIR and WAXD results (see Figs. 2 and 7). In Fig. 10c, no spherulites are seen and the sizes of lamellae are much larger than the lamellae shown in Fig. 10a, which is qualitatively in good agreement with the XRD results (see Table 1). The dark spots in Fig. 10c could be due the presence of very small spherulites or some crystalline parts that have been removed by etching. Applying higher air cooling rate slightly improved the orientation and size of lamellae and for that reason the results are not presented here. Additionally, for the L-AFR condition, it was realized that T_{cast} lower than 100 °C did not noticeably influence the structure of the air cooled films, indicating that the crystal structure has been established before contacting the nip roll. In other words, by applying air cooling, the frost line has been formed before the extruded film touches the nip roll. Therefore, high T_{cast} (i.e. $T_{cast} = 120$ °C or 110 °C) affects the structure as annealing does (i.e. removes the imperfection in crystalline phase and slightly increases the crystal size and orientation [8,18,22]). This is why the films produced under air cooling and high T_{cast} show slightly higher orientation than the ones obtained at low T_{cast} (i.e. $T_{cast} = 100$ °C or lower).

It is well established that the structure of the crystalline and amorphous phases strongly influence the mechanical and tear properties of films. In other words, the mechanical and tear behaviors are closely related to structure changes. Zhang et al. [23] studied the microstructure of LLDPE, LDPE, and HDPE blown films and showed that the type of oriented structure was greatly dependent on the type of polyethylene as well as on the processing conditions. These structure differences were shown to translate into different ratios for MD and TD tear and tensile strengths [23]. Fig. 11a and b shows the typical stress–strain behavior (for samples prepared without and with air cooling) along MD and TD, respectively. The stress–strain response for the no air cooled samples along MD exhibits the typical behavior of films of a spherulitic structure with an elastic response at low deformation, yielding and plastic behavior at medium deformation, and strain hardening at high elongation. In contrast, the stress–strain response of the air cooled specimens along MD reflects the typical behavior of films of a lamellar crystalline morphology with an initial elastic response at low deformation followed by two strain hardening zones. An extensive discussion on this behavior can be found in Samuels [24]. To clearly understand the influences of air cooling on the mechanical properties of the manufactured films, the Young modulus, yield stress, tensile strength, tensile toughness along MD, elongation at break, and yield stress along TD for all the films were determined, as depicted in Figs. 12 and 13, respectively. It is very important to note that all properties along MD (Fig. 12) improve significantly as the films are subjected to a low level of AFR. This can be easily explained by the much better alignment of the lamellae due to air cooling. Additionally, it should be pointed out that further increases of AFR do not noticeably change the mechanical properties along MD, which is in agreement with their orientation trend (see Figs. 2 and 7).

The enhancement of the mechanical response along MD, due to the high orientation of the cooled specimens along MD, was, however, accompanied by significant reductions of the elongation at break along TD (Fig. 13). This anisotropy of the tensile properties along MD and TD was also reported for different PE resins [23] and it was shown that as the level of orientation increased the anisotropy in the mechanical properties increased. Fig. 13 also shows that the yield stress along TD is enhanced as the air flow rate is increased. According to Zhou and Wilkes [25], for HDPE having a stacked lamellar structure, stretching perpendicular to MD caused the crystal lamellae to break up or rupture by chain pull-out. In our case, it is postulated that applying air cooling forms more tie chains between the stacked lamellae, which are possibly responsible for the increase of the yield stress with increasing air flow rate.

Table 2 reports the mechanical properties along MD and TD for the films produced at T_{cast} of 120, 110, 100 °C under N-AFR as well as L-AFR conditions. Compared to the no air cooled films, a significant effect of low air blowing on the mechanical properties, at all drum temperatures, is observed. It is clear that the Young modulus, yield stress, tensile toughness, and tensile strength along MD decrease as T_{cast} decreases. This is due to the formation of more lamellae at higher T_{cast} for the no air subjected films (see Fig. 10a and b) and annealing effect at high T_{cast} for the air subjected films.

It is well understood that tear measurements are very sensitive to the type and alignment of crystalline morphology [23]. Along

Table 2
Mechanical properties of the cast films along MD and TD (the numbers in parenthesis indicate the standard deviation of the measurements); DR = 75.

	Mechanical properties along MD					Mechanical properties along TD	
	Young modulus (MPa)	Yield stress (MPa)	Tensile toughness (MPa)	Strain at break	Tensile strength (MPa)	Yield stress (MPa)	Strain at break
$T_{cast} = 120$ °C, N-AFR	683.5 (61.8)	14.5 (2.7)	93.2 (15.2)	5.5 (0.0)	25.7 (3.1)	20.0 (1.6)	1.2 (0.4)
$T_{cast} = 120$ °C, L-AFR	967.0 (157.0)	26.1 (4.8)	122.7 (25.3)	2.8 (0.4)	53.0 (7.2)	25.7 (6.1)	0.05 (0.01)
$T_{cast} = 110$ °C, N-AFR	604.4 (51.2)	12.2 (2.0)	81.3 (13.6)	6.2 (0.4)	21.3 (7.6)	17.5 (1.3)	1.5 (0.1)
$T_{cast} = 110$ °C, L-AFR	890.2 (98.3)	23.5 (3.3)	106.0 (15.6)	2.7 (0.1)	49.2 (2.4)	25.2 (0.6)	0.05 (0.01)
$T_{cast} = 100$ °C, N-AFR	562.9 (167.5)	10.8 (3.1)	74.6 (15.4)	6.7 (0.1)	19.7 (4.3)	15.9 (0.8)	1.48 (0.1)
$T_{cast} = 100$ °C, L-AFR	853.8 (19.8)	22.1 (1.0)	97.8 (1.8)	2.4 (0.0)	46.9 (0.8)	23.5 (4.9)	0.05 (0.01)

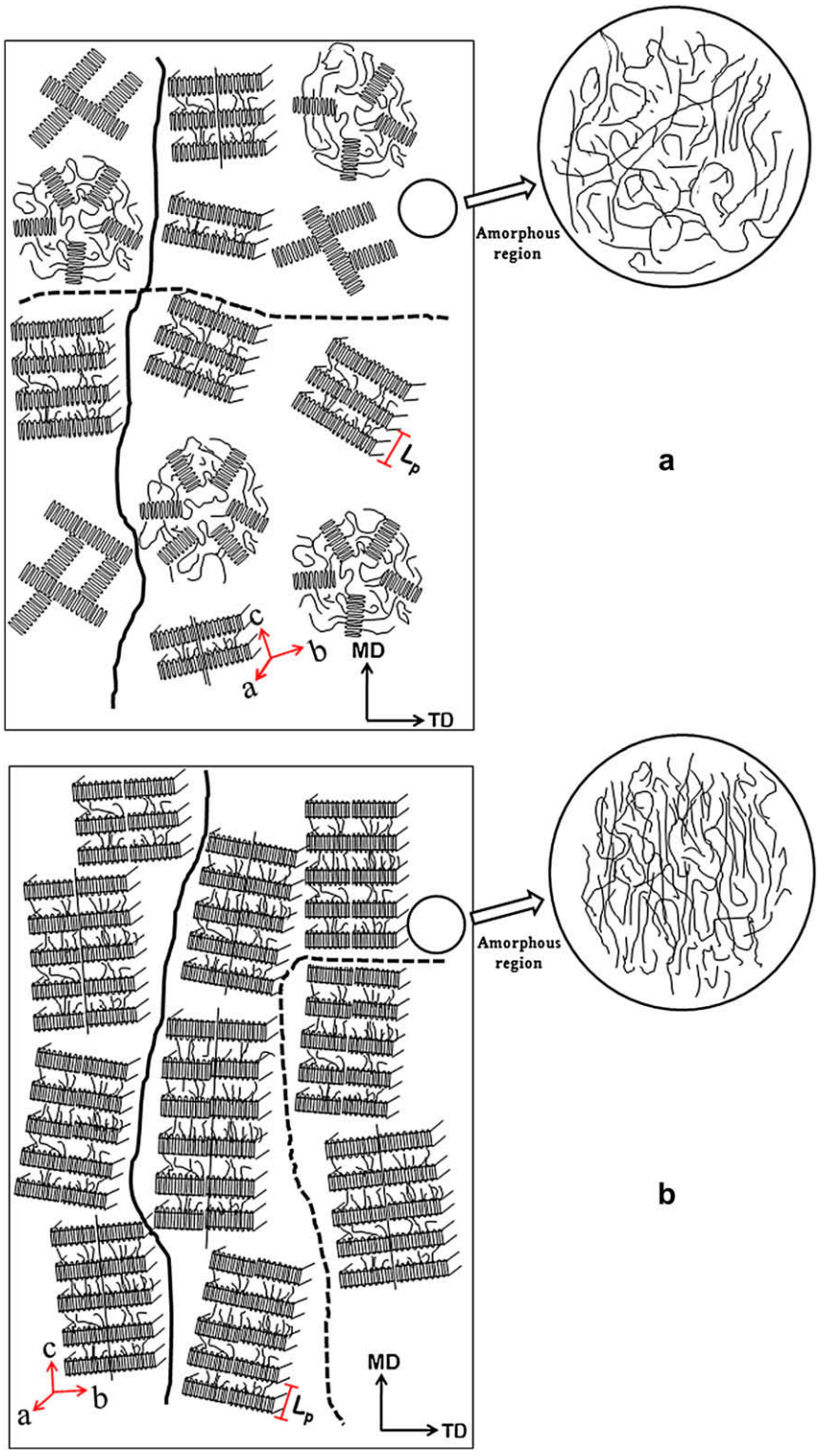

Fig. 14. Proposed pictograms of the molecular structure for: (a) no air cooled cast films and (b) air cooled cast films (the solid lines represent the tear path along MD and the dash lines show the tear path along TD).

MD, tear resistance values of 0.178, 0.154, 0.146, and 0.121 g/μm were measured for the films obtained at $T_{cast} = 120\ ^{\circ}C$ and N-AFR, L-AFR, M-AFR, and H-AFR, respectively: the higher the orientation of the crystalline and amorphous phases, the lower the tear resistance along MD. It was observed that measurements of the tear resistance along TD for samples subjected to air cooling were impossible, because the tearing direction deviated most of the time to MD. In fact, there is a high resistance in TD when compared to MD, which causes a crack in MD and created non-reproducible data that are not reported here. This implies that for air cooled films, a shish–kebab lamellar crystal structure with shishs aligned in MD is formed.

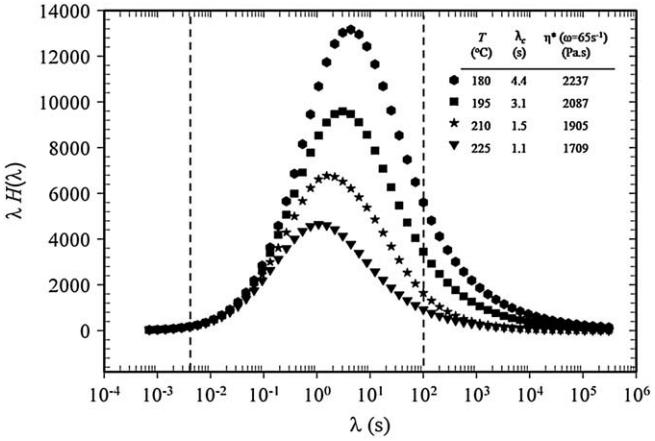

Fig. 15. Weighed relaxation spectra for different melt temperatures (the vertical dash lines represent the range of frequencies covered during the experiments).

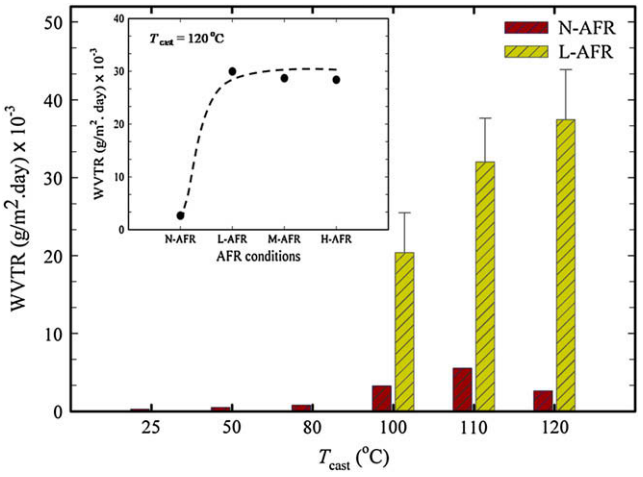

Fig. 17. Water vapor transmission rate (WVTR) as a function of cast roll temperature. The inset is a plot of WVTR as a function of air flow rate condition for $T_{cast} = 120$ °C.

Based on our observations from thermal analysis, FTIR results, WAXD and SAXS patterns, microscopy, mechanical and tear properties, two microstructural pictograms (one for the no air cooled cast film and another for the cast films produced with the use of air cooling) are proposed as depicted in Fig. 14.

For the films produced at high chill roll temperatures and without air cooling, FTIR data, WAXD and SAXS patterns suggest the presence of a lamellar crystalline structure (rows of lamellae and/or cross-hatched), which is not preferentially oriented in MD (see Figs. 2, 7, and 8). Additionally, the facility of tearing these samples along TD indicates that the shishs are not long. However, for these samples, the stress–strain behavior along MD and TD implies the presence of a spherulitic crystalline structure as well. Therefore, as illustrated in Fig. 14a, for the films produced without air cooling and at high T_{cast}, it is believed that spherulitic, row nucleated, and cross-hatched lamellar crystalline structures coexist as confirmed by the SEM micrographs of Fig. 10a and b. In Fig. 14a, the solid line represents the tear path for the sample torn in MD, whereas the dash line reflects the tear path for the one torn in TD. The cast films having this mixed structure can be easily torn along both MD and TD. At low cast roll temperatures (i.e. at temperatures far below T_c of the resin), low orientation values for both crystalline and amorphous phases were determined (see Figs. 2 and 3), indicating the formation of more spherulitic and randomly cross-hatched crystal forms.

In contrast, for the films produced under air cooling, FTIR data, SAXS and WAXD patterns suggest the presence of a stacked lamellar crystal structure, which is preferentially oriented into MD (see Figs. 2 and 7). In addition, the impossibility to tear these samples along TD suggests that the size of the shish is much larger in comparison with those for the films casted under N-AFR. Furthermore, a very low elongation at break along TD for the films subjected to air cooling is an indication that the spherulitic crystalline structure does not exist or is present in a very small quantity. This is confirmed by the SEM results shown in Fig. 10c. Hence, as depicted in Fig. 14b, a uniform shish–kebab structure for the films produced under air cooling is expected. The cast films having this structure can be easily torn along MD. However, as sketched in Fig. 14b, because of the presence of the long shishs, tearing along TD is impossible and the tearing direction always deviates to MD. As described before, under air cooling conditions, the variation of T_{cast} does not noticeably affect the shish–kebab structure.

Based on FTIR results for the orientation of the amorphous phase (see Fig. 3), circles in Fig. 14a and b also reveal the proposed structure for the amorphous region of films made without and upon air cooling, respectively. By applying air cooling, the extruded film temperature at the die exit decreases and, as a consequence, the applied stress on the polymer chains increases. This yields some local organization in the amorphous phase, which is responsible for its higher orientation.

In the following section, justifications regarding the roles of air cooling and drum temperature on the final crystal microstructures are presented. The orientation and morphological differences are believed to originate from the rheological characteristics and crystallization kinetics. It is well-known that temperature has a crucial

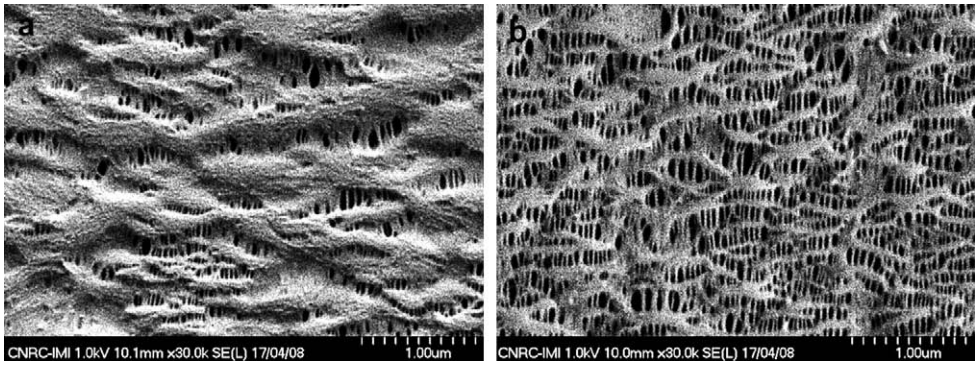

Fig. 16. SEM micrographs of the surface of the films obtained at: (a) N-AFR and (b) L-AFR; $T_{cast} = 120$ °C and DR = 75, cold stretching of 35%, followed by hot stretching of 55%. MD ↑ and TD →.

effect on the relaxation time of polymer chains as well as on the crystallization rate. In order to consider the effects of temperature on the applied stress and relaxation time of the molecules, linear dynamic rheological measurements were carried out. Fig. 15 reports the weighted relaxation spectra for different melt temperatures using the NLREG (non linear regularization) software [26] (the vertical dash lines represent the range of frequencies covered during the experiments). We considered the characteristic relaxation time, λ_c, corresponding to the peak of the curves. From Fig. 15, as temperature is decreased a longer relaxation time is observed (see the legend in figure). Assuming a linear velocity profile for the melt film between the die exit and cast roll nip and also assuming pure uniaxial flow in this region, the effective deformation rate based on the second invariant of the rate-of-deformation tensor was estimated to be around 65 s^{-1}. The complex shear viscosities at 65 s^{-1} and for different temperatures were taken as estimates of the melt viscosity and their values are reported in the legend of Fig. 15. Obviously, the lower the temperature the larger the viscosity, and consequently the higher the applied stress. Hence, as air cooling is used, the melt temperature right at the exit of the die decreases and, as a consequence, the applied stress (or relaxation time) rises drastically. This promotes the number of shishs or nuclei sites, resulting in a noticeable increase of the probability for the formation of lamellae by the low molecular weight chains.

In general, the rate of crystallization is first controlled by nucleation and then by the growth and packing of the crystals [27]. In our case, the air cooling causes a large decrease in the extruded film temperature such that crystallization temperature of the resin is reached before the frost line is formed. This increases the number of nuclei sites resulting in a much faster crystallization rate. This fact, together with the intrinsic temperature effects on the relaxation time, as discussed above, determines a significant coupling between temperature and flow, yielding to a novel highly oriented lamellar structure. In other words, the use of air cooling in addition to chill rolls in the cast film process helps flow induced crystallization to occur at lower temperatures. This will noticeably increase the number of shish or nuclei sites, and consequently the crystallization kinetics is promoted resulting in a well oriented shish–kebab structure.

To produce microporous membranes by the stretching technique, precursor films with an adequate orientation and alignment of the crystal lamellae are needed [9,18]. In this study, the effects of microstructure differences of the PP cast films on the microporous membranes morphology and water vapor transmission rate were investigated. Three consecutive stages were carried out to obtain porous membranes: cast or precursor film formation, annealing, and stretching in two steps (cold and hot). During cold stretching, the pores were created whereas in the subsequent hot stretching they were enlarged. WAXD and FTIR measurements clearly showed that cooling drastically enhanced orientation of the crystal lamellae in the precursor films; hence, a microporous membrane with more pore density and better tortuosity is expected as air cooling is utilized.

Fig. 16 presents SEM micrographs of the surface of the fabricated membranes. Very thick lamellae, non uniform pores and a small amount of pores for the porous membrane obtained from the no air cooled film is observed (Fig. 16a). However, for the membrane prepared from the cast film subjected to a small air cooling rate, the number of pores noticeably increases and more uniform pore sizes and a better morphology are observed (Fig. 16b). Note more and thinner lamellae appear for the latter compared to the former, supporting the previous results.

Fig. 17 presents the water vapor transmission rates (WVTR) of the produced microporous membranes. Small WVTR values were recorded for the no air cooled samples produced at different cast roll temperatures. However, interestingly, the WVTR increased by a factor of 20 when the film surface was subjected to a low air flow, which is attributed to the formation of more pores, higher porosity, and better interconnection between the pores. Compared to the sample prepared at L-AFR, further increases of the air cooling rate (i.e. at M-AFR and H-AFR) did not significantly increase the permeability was (see the inset of Fig. 17), indicating that more air cooling does not dramatically influence the lamellar structure, in accordance with the previous results (see Figs. 2–8).

4. Conclusions

In this work, we have investigated the structure of polypropylene cast films made under different air cooling conditions, chill roll temperatures, and draw ratios. Our findings can be summarized as follows:

- In the cast film process, air cooling and cast roll temperature had a crucial role on the orientation of the crystalline as well as the amorphous phases.
- Increasing the draw ratio increased the crystal orientation (F_c), and a stronger effect of the draw ratio on F_c was observed by applying air cooling.
- The use of a low air cooling rate contributed significantly to the perfection of the crystalline phase, while further increasing of air cooling did not noticeably affect the crystal structure.
- Significant increases of the Young modulus, yield stress, tensile strength, and tensile toughness along MD, and dramatic decreases of elongation at break along TD were observed as air cooling was applied. These were explained by a better molecular and crystal orientation for air cooled cast films.
- For films produced without air cooling and at high roll temperature, coexisting lamellae and spherulites were observed. In contrast, an ordered stacked lamellar structure was seen for the films subjected to a low air cooling.
- Better orientations of the crystalline and amorphous phases for the air cooled films were attributed to the larger relaxation time and faster flow induced crystallization. Applying air cooling in addition to the use of cast rolls helped flow induced crystallization to occur at lower temperatures. This noticeably increased the crystallization kinetics, resulting in a well oriented shish–kebab structure.
- Microporous membranes having high pore density, large porosity, and high water vapor permeability were obtained by lamellae separation for cast films prepared using air cooling.

Acknowledgements

Financial support from NSERC (Natural Science and Engineering Research Council of Canada) and from FQRNT (Fonds Québécois de Recherche en Nature et Technologies) is gratefully acknowledged. We also acknowledge the large infrastructure grant received from the Canadian Foundation for Innovation (Government of Canada and Province of Quebec), which allowed us to build the unique POLYNOV facility. We are also thankful to Messrs. P. Cigana, L. Parent and P.M. Simard for their technical help. Finally, we are thankful to ExxonMobil who donated the resin used in this work.

References

[1] Ajji A, Zhang X, Elkoun S. Polymer 2005;46:3838–46.
[2] Coppola S, Balzano L, Gioffredi E, Maffettone PL, Grizzuti N. Polymer 2004;45:3249–56.
[3] Doufas AK, Dairanich IS, Mchugh AJ. J Rheol 1999;43:85–109.
[4] Doufas AK, Mchugh AJ. J Non-Newtonian Fluid Mech 2000;92:81–103.
[5] Swartjes FHM. Stress induced crystallization in elongational flow, PhD thesis, Technische Universiteit Eindhoven; 2001.
[6] Agarwal PK, Somani RH, Weng W, Mehta A, Yang L, Ran S, et al. Macromolecules 2003;36:5226–35.

[7] Somani RH, Hsiao BS, Nogales A, Srinivas S, Tsou AH, Sics I, et al. Macromolecules 2000;33:9385–94.
[8] Somani RH, Yang L, Hsiao BS. Polymer 2006;47:5657–68.
[9] Tabatabaei SH, Carreau PJ, Ajji A. J Membr Sci 2008;325:772–82.
[10] Fujiyama M, Inata H. J Appl Polym Sci 2002;84:2157–70.
[11] Sadeghi F, Ajji A, Carreau PJ. Polym Eng Sci 2007;47:1170–8.
[12] Alexander LE. X-ray diffraction methods in polymer science. New York: Wiley Inter Science; 1969.
[13] Arroyo M, Lopez-Manchado MA. Polymer 1997;38:5587–93.
[14] Olley RH, Bassett DC. Polymer 1982;23:1707–10.
[15] Koerner H, Kelley JJ, Vaia RA. Macromolecules 2008;41:4709–16.
[16] Kawakami D, Burger C, Ran S, Avila-Orta C, Sics I, Chu B, et al. Macromolecules 2008;41:2859–67.
[17] Macro Y, Chevalier L, Chaouche M. Polymer 2002;43:6569–74.
[18] Sadeghi F, Ajji A, Carreau PJ. J Membr Sci 2007;292:62–71.
[19] Klug HP, Alexamder LE. X-ray diffraction procedures. New York: John Wiley & Sons; 1954.
[20] Somani RH, Yang L, Zhu L, Hsiao BS. Polymer 2005;46:8587–623.
[21] Guinier A, Fournet G. Small-angle scattering of X-rays. New York: Wiley; 1955.
[22] Hedesiu C, Demco DE, Kleppinger R, Buda AA, Blumich B, Remerie K, et al. Polymer 2007;48:763–77.
[23] Zhang XM, Elkoun S, Ajji A, Huneault MA. Polymer 2004;45:217–29.
[24] Samuels RJ. J Polym Sci Polym Phys Ed 1979;17:535–68.
[25] Zhou H, Wilkes GL. J Mater Sci 1998;33:287–303.
[26] Honerkamp J, Weese J. Rheol Acta 1993;32:65–73.
[27] Tian J, Yu W, Zhou C. J Appl Polym Sci 2007;104:3592–600.